Point-defect computer simulation including angular forces in bcc iron

G. Simonelli, R. Pasianot, and E. J. Savino
Departamento Ciencia de Materiales, Comisión Nacional de Energía Atómica, Avda. Libertador 8250, (1429) Buenos Aires, Argentina
(Received 6 October 1993; revised manuscript received 28 March 1994)

An embedded-defect (ED) interatomic potential for Fe is presented. The ED model is based on the same physical description of interactions as the embedded atom method (EAM) but including angular-dependent many-body local terms. In this work, the ED potential is fitted to several Fe properties and is used to simulate the vacancy and various self-interstitial configurations. The pair and many-body contributions to the formation energy of the defects are calculated, as well as the corresponding relaxation volumes. The results are compared to those obtained with an EAM potential fitted to the same properties. The vacancy displacement field is studied in detail for both potentials. Anharmonic effects are assessed and correlated with the unrelaxed force pattern.

I. INTRODUCTION

Several empirical or semiempirical interatomic potentials that include many-body interaction terms have been developed recently. They enable one to overcome some shortcomings of the pair interaction model, widely used in computer simulation studies in the past. Their goal is to account for the delocalized physical nature of the metallic bonding while retaining the calculation simplicity of pair potentials. Among the first of these approaches was the embedded-atom method (EAM) of Daw and Baskes,[1] the *N*-body potentials of Finnis and Sinclair,[2] and the glue model of Ercolessi, Tosatti, and Parrinello.[3] All of them proposed a pair interaction plus an electronic (or atomic) density-dependent term for the description of the energy associated with each atomic site. Within the same spirit, but including some aspects of bond directionality, other models have been developed; among them, the modified embedded-atom method[4] (MEAM), the embedded defect[5] (ED), and Carlsson's potentials for bcc metals.[6]

The physical basis behind empirical interatomic potentials has been reviewed and discussed by Carlsson in Ref. 7, where they are classified in pair potentials, pair functionals, cluster potentials, and cluster functionals, depending on how the many-body interactions are expanded. Interatomic potentials in the EAM approximation correspond to pair functional expansions of the energy. They are known to fail, for instance, in the prediction of structural energies. Furthermore, whenever covalent or angle-dependent interactions are important, the application of this model is questionable. As argued in Ref. 8, this is possibly the case of bcc metals. Therefore the influence of higher-order many-body terms for describing interactions in these materials must be systematically studied.

In Ref. 5, Pasianot, Farkas, and Savino deduced the ED potential, an empirical many-body potential for bcc transition metals. There, the energy was expanded following the spirit of the EAM, but adding a dipolelike-dependent functional. Heuristically, this procedure is equivalent to embedding every atom as a defect on the otherwise homogeneous electron density (as in the EAM), but including a dipole contribution to the configuration energy. Baskes' first version of the MEAM (Ref. 9) is quite similar to the ED approximation, while in later versions other second- and higher-order terms are included.[4,10]

An EAM and an ED potential for Fe are used here for the simulation of point defects, namely, the single vacancy and several interstitial configurations. In Ref. 5, EAM and ED potentials for several bcc metals were given. Some analytic features of the EAM-type potential for Fe were improved by Simonelli, Pasianot, and Savino in Ref. 11, making it more adequate for computer simulation studies. There, point-defect simulations were performed, and the most suitable interaction range was obtained by fitting the experimental results. The EAM potential used here is the short-range potential from Ref. 11, which includes up to second-neighbor interactions. On the other hand, the ED potential constructed in this work is fitted to the same Fe properties and keeping the same interaction range.

The results for either potential are carefully analyzed and compared among themselves and with others from the literature.[12–15] It is shown that the display of the bare displacement field obtained from the computer simulation does not reveal some subtleties of the potential employed, and therefore a more refined analysis is presented in order to judge among different potentials. Savino and Farkas[16] have compared simulation results using the harmonic Green function approximation and the concept of a force source for understanding some of the important features on surface relaxation. Because of its simplicity, the vacancy problem is the ideal candidate for comparing results and for testing the reliability of the interatomic potentials. Although for the vacancy the harmonic model has been developed by several authors and related to pair potential predictions, e.g., Tewary,[17] theoretical development is still needed when many-body potentials, and eventually large anharmonicity at the defect core, are considered.

The purpose of this work is then twofold: On the one hand, an improved ED potential for Fe with respect to

the one in Ref. 5 is reported, and on the other, the differences arising in the simulations of point defects when many-body angular terms are included are analyzed by comparing the results obtained with the EAM and ED potentials.

In Sec. II the ED model and the potential fitting procedure are presented. In Sec. III we describe the defect calculation method for the computer simulation and the harmonic approximation, paying special attention to the single-vacancy case. Results of the vacancy simulation (lattice distortion, formation energy, and relaxation volume) are given in Sec. IV, as well as an analysis of the forces around that defect. In Sec. V calculations for self-interstitials are presented, and in Sec. VI, the results of this work are discussed.

II. INTERATOMIC POTENTIALS

Within the ED method proposed in Ref. 5, the energy E_i at a site i is expanded as

$$E_i=\frac{1}{2}\sum_{j\neq i}V(R_{ij})+F(\rho_i)+G(Y_i)\ . \tag{1}$$

The first term $V(R_{ij})$ represents a pair interaction; it depends on the distance R_{ij} between atoms i and j. The many-body terms $F(\rho_i)$ and $G(Y_i)$ depend on invariants of the tensor λ_i defined at each atomic site as

$$\lambda_i^{\alpha\beta}=\sum_{j\neq i}\Phi(R_{ij})R_{ij}^{\alpha}R_{ij}^{\beta}/R_{ij}^2\ , \tag{2}$$

where R_{ij}^{α} denotes the α component of the vector joining atoms i and j, and Φ is a function of the distance between these atoms. The arguments ρ_i and Y_i are given by

$$\rho_i=\mathrm{Tr}\lambda_i=\sum_{j\neq i}\Phi(R_{ij}) \tag{3}$$

and

$$Y_i=\sum_{\alpha,\beta}\lambda_i^{\alpha\beta}\lambda_i^{\alpha\beta}-\rho_i^2/3\ . \tag{4}$$

Thus, taking Φ as an atomic electron density, the term $F(\rho_i)$ is analogous to the embedding function of the EAM. The other term $G(Y_i)$ is angle dependent due to Eq. (4). Note that the calculation of the tensor λ_i is straightforward, since it involves pair sums only. Also note that $Y_i=0$ for cubic symmetry.

Without loss of generality, we impose the many-body part of the energy $F(\rho_i)$ in Eq. (1) to have a null first derivative at the equilibrium perfect lattice. In addition, the term $G(Y_i)$ does not contribute to the force equilibrium and zero-pressure conditions in a cubic lattice [Eqs. (13) and (21) in Ref. 5], therefore $V(R_{ij})$ is an effective pair interaction potential,[2] i.e., it holds in equilibrium a lattice with the correct lattice parameter.

The potential is fitted to the Fe bcc lattice parameter, the elastic constants, an estimated value for the unrelaxed vacancy formation energy $E_f^{v,NR}$, and the cohesive energy E_{coh} (through Rose's equation of state[18]). Experimental values for these properties are shown in Table I. Explicit equations to fit ED potentials for cubic Bravais lattices are reported in Ref. 5. For the sake of completeness, we shall describe here the main steps of the procedure and present the functional form chosen for the energy expansion terms, as well as the values of the parameters obtained.

The first step consists of fixing the electron density function Φ. We choose a Thomas-Fermi-like screening function. Equation (22) of Ref. 5 is smoothly matched to zero according to

$$\Phi(x)=\begin{cases}\exp(-\beta x)/x\ , & x\leq x_1\ ,\\ (x-x_2)^3(h_0+h_1x+h_2x^2)\ , & x_1<x\leq x_2\ ,\\ 0\ , & x>x_2\ ,\end{cases} \tag{5}$$

where $\beta=5$ and x is in units of the equilibrium first-neighbor distance. The adequate cutoff is obtained by fixing x_1 and x_2 and calculating the coefficients h_i that make the function and its first two derivatives continuous at those points.

On constructing ED potentials, an arbitrary relative contribution of the terms F and G to the energy must be imposed. The parameter selected for this purpose is ξ, the relative contribution of the many-body terms to the unrelaxed vacancy formation energy ($E_f^{v,NR}$). If only first and second neighbors are considered,

$$\xi E_f^{v,NR}=8F(\rho_1)+6F(\rho_2)-14F(\rho_0)+8G(Y_1)+6G(Y_2)\ , \tag{6}$$

where the subindexes 1 and 2 refer to the functions evaluated at the neighboring shells 1 and 2 from the vacancy and 0 stands for the perfect lattice configuration ($\rho_0=1$ and $Y_0=0$ in our model). An approximate expression is used for ξ, assuming that the differences between perfect and defect values for the arguments ρ_i and Y_i are small,[5]

$$\xi E_f^{v,NR}=(\tfrac{1}{2}F_0''+\tfrac{2}{3}G_0')\sum_{\nu}N_\nu\Phi_\nu^2\ , \tag{7}$$

where $F_0''=(d^2F/d\rho^2)_{\rho=\rho_0}$, $G_0'=(dG/dY)_{Y=Y_0}$, ν is the index of the atomic shell around the vacancy, and N_ν is the number of atoms in that shell. On the other hand, the equation for the Cauchy pressure is[5]

$$\Omega\frac{c_{12}-c_{44}}{2}=\tfrac{1}{2}F_0''P_1^2-\tfrac{1}{6}G_0'(2P_2^2+3P_3^2)\ , \tag{8}$$

where P_i^2 are functions of Φ only. Since this latter func-

TABLE I. Data fitted by the EAM and ED potentials. Elastic constants are in eV/Å^3.

Ω (Å^3)	a (Å)	E_{coh} (eV)	$E_f^{v,NR}$ (eV)	$(c_{11}+2c_{12})/3$	$(c_{11}-c_{12})/2$	c_{44}
11.78	2.866	4.28[a]	1.8	1.113[b]	0.298[b]	0.699[b]

[a]Reference 19.
[b]Reference 20.

TABLE II. ξ is the many-body contribution to the vacancy formation energy and θ_1, θ_2, and θ_3, the resulting many-body contributions to the bulk modulus $(c_{11}+2c_{12})/3$ and to the shear modulii $(c_{11}-c_{12})/2$ and c_{44}, respectively.

	ξ	F_0'' (eV)	G_0' (eV)	θ_1	θ_2	θ_3
EAM	0.013	1.65		0.193	0.000	0.000
ED	0.200	3.51	5.66	0.410	0.013	0.341

tion is chosen beforehand, Eqs. (7) and (8) define a system of two linear equations with G_0' and F_0'' as unknowns. From Eq. (8), it is clear that the inclusion of $G(Y_i)$ is strictly needed only when $(c_{12}-c_{44})<0$ ($F_0''>0$, $G_0'>0$ on physical grounds), which is not the case for Fe. In the EAM approach, $G_0'=0$ in the above equations; therefore, F_0'' and ξ are fixed through Eqs. (8) and (7), respectively. In the ED method, for a chosen value of ξ, G_0' and F_0'' are determined by solving the system of Eqs. (7) and (8), and the relative contributions of the many-body terms to the elastic constants can be calculated. We choose $\xi=0.2$ for the ED potential, resulting 0.03 from the term F_0'' and 0.17 from G_0'. As mentioned before, ξ is not fixed in advance for the EAM potential; the value $\xi=0.013$ is obtained, implying a different contribution of the many-body terms to the elastic constants in each potential. These relationships are reported in Table II. In that table $\theta_1,\theta_2,\theta_3$ stand, respectively, for the relative contribution of the many-body part of the potential to the bulk modulus $B=(c_{11}+2c_{12})/3$ and to the shear modulii $(c_{11}-c_{12})/2$ and c_{44}.

For the effective pair potential we propose:[21]

$$V(x)=\sum_{i=1}^{4} a_i(x-z_i)^3 H(z_i-x)\ , \tag{9}$$

with

$$H(z_i-x)=\begin{cases}1\ , & x\le z_i\ ,\\ 0\ , & x>z_i\ ,\end{cases}$$

where the a's are obtained following the procedure of Ref. 11, through satisfaction of the zero-pressure condition and the fitting of the remaining contributions to the elastic constants and to the unrelaxed vacancy formation energy.

$F(\rho)$ is obtained numerically by fitting the equation of Rose *et al.*[18] Note that Y remains null in a uniform expansion or compression of the crystal; therefore,

$$F(\rho_i)=E(\bar{a})-\frac{1}{2}\sum_{j\neq i} V(R_{ij})\ , \tag{10}$$

where $E(\bar{a})$ is given by

$$E(\bar{a})=-E_{\rm coh}(1+\bar{a})\exp(-\bar{a}) \tag{11}$$

and where $\bar{a}=\alpha(R_1/R_{1e}-1)$, with R_{1e} the equilibrium value of the first-neighbor distance R_1, $\alpha^2=9\Omega B/E_{\rm coh}$, and Ω the atomic volume.

Finally, following Ref. 5, a linear approximation for the term $G(Y)$ is proposed, i.e., $G(Y)=G_0'Y$. Therefore the ED potential can be considered as a first-order expansion of the EAM in the variable Y. The approximation is satisfactory whenever the argument Y does not differ much from its perfect lattice value, but this condition may not be fulfilled in the neighborhood of "strong" defects. Other lattice properties besides those considered here must be fitted in order to obtain a more adequate dependence of the energy on this variable.

The complete set of parameters for the Fe ED potential is given in Table III. We also report there the parameters corresponding to the EAM potential used in this work (the short-range potential presented in Ref. 11) and the predicted energy differences between the bcc structure and the more compact hcp and fcc ones. As mentioned before, all functions have the same interaction range in order to allow for a consistent comparison.

III. POINT-DEFECT LATTICE RELAXATION

A. Computer simulation

Vacancy and self-interstitial configurations are simulated using the interatomic potentials reported in the previous section. The simulations are performed for a spherical block of ~1500 free atoms (region I) for the vacancy and ~9000 for the interstitial configurations, surrounded by atoms fixed at their perfect lattice positions (region II)

TABLE III. Parameters of the potentials fitted to bcc-iron properties. $z_4(=x_2)$ is the interaction range. The length unit is the first-neighbor distance in equilibrium. $\rho=1$ for the perfect lattice in equilibrium. Coefficients a are in eV. The function $F(\rho)$ is obtained numerically (see text).

		EAM	ED
Function Φ	x_1	1.10	1.10
	x_2	1.40	1.40
	h_0	−53.553 74	−53.553 74
	h_1	101.830 17	101.830 17
	h_2	−49.935 30	−49.935 30
Function V	z_0	0.999	
	z_1	1.020	1.020
	z_2	1.030	1.030
	z_3	1.380	1.380
	z_4	1.400	1.400
	a_0	−60.000 00	
	a_1	94.416 05	−236.016 63
	a_2	−45.226 89	198.410 45
	a_3	−139.686 02	−120.160 72
	a_4	124.058 56	106.308 96
Function G			$G_0'=5.66$ eV
$E_{\rm fcc}-E_{\rm bcc}$		0.007 eV/atom	0.015 eV/atom
$E_{\rm hcp}-E_{\rm bcc}$		0.007 eV/atom	0.015 eV/atom

and interacting with the inner ones. Though a smaller block size can be used to simulate the interstitial configurations, the chosen size is needed to perform an adequate analysis of defect core anharmonicity that will be reported elsewhere. Such an analysis for the single vacancy is given in sections below. A conjugate gradient code, based on DEVIL,[22] is employed to determine the configuration that minimizes the energy. Formation energies and relaxation volumes are calculated, and the contributions of the pair and the many-body terms are reported separately.

The defect formation energy (E_f) is obtained as the difference between the energy of a lattice consisting of N sites in region I with the defect at its center and the energy of a perfect lattice with the same number of atoms ($N-1$ in the case of a vacancy and $N+1$ for a self-interstitial) for N sufficiently large:

$$E_f=\lim_{N\to\infty}\{E^{N\pm1}(\bar{r}^D)-E^{N\pm1}(\bar{r}^0)\}\ , \tag{12}$$

$\bar{r}$ being a vector of dimension $3(N\pm1)$: $\bar{r}=(\mathbf{R}_0,\ldots,\mathbf{R}_{N\pm1})$, with $\mathbf{R}_i$ the position of atom i; $\bar{r}^D$ corresponds to the defect configuration and $\bar{r}^0$ to the perfect lattice one. Because of the additive property of the energy, expressed in Eq. (1), it is possible to separate in Eq. (12) the contribution of each term of Eq. (1). For instance, the pair contribution is given as

$$E_{f,\text{pair}}=\lim_{N\to\infty}\left\{\frac{1}{2}\sum_{i=1}^{N\pm1}\sum_{j\neq i}V(R_{ij}^D)-\frac{N\pm1}{2}\sum_{j\neq i}V(R_{ij}^0)\right\}\ , \tag{13}$$

where the last term does not depend on the subindex i.

The lattice distortion can be pictured, besides the displacement field, by the parameters $\tilde{\rho}$ and $\tilde{Y}$, which are related to the arguments of the many-body functions F and G, respectively, and defined at each site i as

$$\begin{aligned}\tilde{\rho}_i&=\rho_i-1\ ,\\ \tilde{Y}_i&=\sqrt{(3/5)Y_i}\ .\end{aligned} \tag{14}$$

$\tilde{\rho}$ gives local density changes, while $\tilde{Y}$ takes account of angular distortions (departure from cubic symmetry). Their special form is related to scaling purposes.

The relaxation volume of the defect, ΔV, is obtained through the corresponding dipole tensor P. In a computer simulation study, the latter quantity can be calculated by the first moment of the forces on the (fixed) atoms in region II:[23]

$$P^{\alpha\beta}=\sum_{j\in\text{II}}R_j^\alpha F_j^\beta\ , \tag{15}$$

which approaches a limiting value as the size of region I increases and encloses the whole defect anharmonicity. Then[24]

$$\Delta V=\text{Tr}(P)/3B\ , \tag{16}$$

where B is the bulk modulus.

B. Harmonic approximation and Kanzaki forces

Flinn and Maradudin[25] and Tewary[17] developed a Green function approach for the calculation of the lattice distortion produced by point defects based on an earlier work by Kanzaki.[26] An extension of their approach was developed in Ref. 16 and used for the understanding of atomic relaxations in computer simulation runs. Within the Green function theory, it is assumed that every atom of the perfect lattice is displaced a small amount $\mathbf{u}_i$ as a consequence of interaction with the defect,

$$\mathbf{R}_i^D=\mathbf{R}_i^0+\mathbf{u}_i\ . \tag{17}$$

Therefore the formation energy can be expanded as a function of the displacements:

$$E_f=E_f^{NR}+\Delta E_f^R\ , \tag{18}$$

where E_f^{NR} is the energy of the ensemble when every atom is located at the perfect lattice position, i.e., the unrelaxed formation energy, and ΔE_f^R stands for the energy relaxation produced by the displacements. In a harmonic approximation,

$$\Delta E_f^R=\lim_{N\to\infty}\sum_{i=1}^{N\pm1}\sum_{\alpha=1}^{3}\left\{-K_i^{0\alpha}u_i^\alpha+\frac{1}{2}\sum_{j=1}^{N\pm1}\sum_{\beta=1}^{3}\phi_{ij}^{*\alpha\beta}u_i^\alpha u_j^\beta\right\}\ , \tag{19}$$

where

$$K_i^{0\alpha}=-\partial E_f/\partial u_i^\alpha \tag{20}$$

is the α component of the force exerted by the defect at the unrelaxed lattice site i and ϕ^* the force constant matrix for the lattice with the defect. The latter can be expressed as

$$\phi^*=\phi+\zeta\ , \tag{21}$$

where ϕ is the force constant matrix corresponding to the perfect lattice and ζ takes account of changes in the constants caused by the defect. The displacement field, obtained by minimizing Eq. (19), is given by

$$u_i^\alpha=\sum_{j,\beta}G_{ij}^{*\alpha\beta}K_j^{0\alpha}\ , \tag{22}$$

where G^* is the Green function matrix of the lattice with the defect, defined as the inverse of the corresponding force constant matrix, $G^*=(\phi^*)^{-1}$. Equation (22) can also be written as

$$u_i^\alpha=\sum_{j,\beta}G_{ij}^{\alpha\beta}K_j^\beta\ , \tag{23}$$

where $G=\phi^{-1}$ is the perfect lattice Green function, related to G^* according to Dyson's formula[17]

$$G^*=G(1+\zeta G^*) \tag{24}$$

and

$$\mathbf{K}=\mathbf{K}^0+\zeta\mathbf{u} \tag{25}$$

are the forces exerted by the defect at the relaxed atomic positions. These are the so-called Kanzaki forces.[26]

The procedure outlined above solves the problem of finding the relaxed defect configuration for a harmonic lattice. At the core region, where the harmonic approximation breaks down, computer simulation techniques can be used for finding the relaxed defect structures. However, the concept of Kanzaki forces is still useful to characterize the defect configuration; it is now *defined* as the forces that in a harmonic approximation produce the same displacements in the lattice as does the defect.[24] This is realized by inversion of Eq. (23) according to

$$K_i^\alpha = \sum_{j,\beta} \phi_{ij}^{\alpha\beta} u_j^\beta , \tag{26}$$

where u_j^β is the (known) result of a computer simulation run. One must remember that the Kanzaki forces so generalized are always exerted on a harmonic lattice.

In terms of the Kanzaki forces, the dipole tensor P of Eq. (15) can also be calculated as[23]

$$P^{\alpha\beta} = \sum_{j=1}^{\infty} R_j^\alpha K_j^\beta . \tag{27}$$

In fact, agreement between Eqs. (15) and (27) is a way to judge if the size of the atomic array employed in the simulation is enough to include all the defect anharmonicity.

C. Core Kanzaki forces

In this section, a procedure is proposed for calculating the Kanzaki forces from the computer simulation displacements at the point-defect core. For this method, knowledge of the force constant matrix of the perfect lattice according to Eq. (26) is not needed. It is also a helpful tool for determining the size of the anharmonic region surrounding the defect.

Kanzaki forces are obtained by computing the gradient of the defect-host interaction potential. This is most easily done using a method devised by Kanzaki,[26] shown schematically in Fig. 1 for the single-vacancy case. That author assumes to know the defect relaxed lattice configuration, i.e., the configuration of minimum energy [Fig. 1(c)] and defines a new lattice where the missing atom is replaced at its perfect lattice site [Fig. 1(b)]. The defect-host interaction potential is defined as the energy difference between configurations (c) and (b), i.e., as $E(c)-E(b)$. In Kanzaki's model, the lattice responds harmonically and the defect core is restricted only to the missing atom. However, in some cases, even for relatively weak defects such as the vacancy, anharmonic effects extend over a larger region. An alternative and general procedure can be used for those cases. The process of Fig. 1(b) is generalized to the one of Fig. 1(d); namely, not only the missing atom, but also largely displaced ones are restored at their perfect lattice position. Forces are evaluated at these restored atomic positions and at the remaining displaced coordinates. The procedure entails defining the defect core as the region where the relevant anharmonic behavior occurs, while the rest of the lattice is essentially harmonic. The method can be carried out to successive degrees of approximation. For instance, the zeroth order of approximation for the vacancy is to consider the defect as represented by the only one missing atom, as Kanzaki did; first order will include first neighbors to the vacant site into the core region; and so on. The Kanzaki forces calculated by the above procedure can be replaced in Eq. (27) to obtain the dipole tensor and from this the defect volume change is computed according to Eq. (16). Eventually, convergency to the dipole tensor value calculated by computer simulation [Eq. (15)] is reached and the defect core region can be consistently defined.

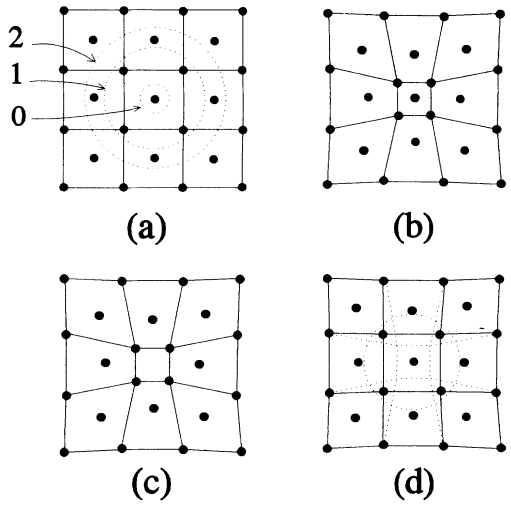

FIG. 1. Kanzaki's scheme to evaluate the defect-host interaction on a planar fcc lattice. (a) Perfect lattice; 0,1,2 label the atomic shells that constitute the defect core in the zeroth, first, and second order of approximation. (b) Relaxed lattice with the vacant atom restored. (c) Distortion induced by the vacancy. (d) Extended scheme to first order (see text).

Note that the above process is, in a sense, symmetric to the one entailed by Eq. (15), but with opposite meaning for regions I and II. Here region I is a perfect rigid lattice and region II contains the (harmonic) displacements of an unbounded solid with the defect at its center; the Kanzaki forces are concentrated on a shell including the boundary between regions I and II.

IV. VACANCY

A. Computer simulation

The vacancy-induced radial displacements resulting from the computer simulation using the EAM and ED potentials are shown in Fig. 2 as a function of the neighboring shell index. We observe that radial displacements are qualitatively similar for both potentials, the main differences being a smaller value for the closest neighbors using the ED potential and larger for the remaining neighbors in the $\langle 111 \rangle$ direction (fifth and tenth shells). As shown later, this behavior is consistent with the magnitude of the total unrelaxed forces.

The lattice distortion according to the many-body parameters defined by Eqs. (14) are represented in Figs. 3(a) and 3(b) for the relaxed configurations obtained with both

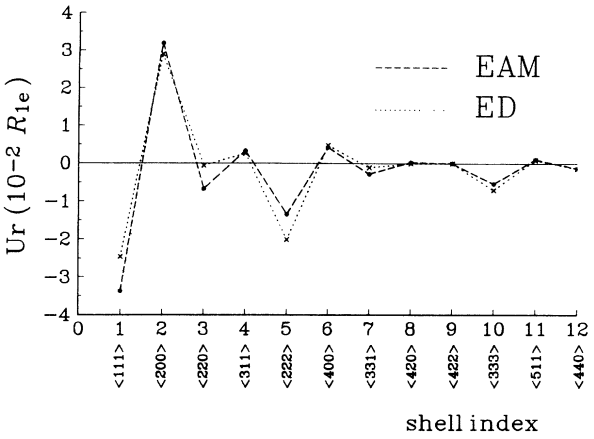

FIG. 2. Vacancy radial displacement as a function of the neighboring shell to the vacancy for both potentials EAM and ED. R_{1e} is the nearest-neighbor distance.

potentials. An oscillatory behavior of the density $\tilde{\rho}$ as a function of neighbor distance is observed. Excluding the defect's closest neighbors, these oscillations in density follow the displacement field pattern reported in Fig. 2; such a behavior is expected since we have chosen a monotonically decreasing electronic function [Eq. (5)]. After the fourth-neighbor atomic shell, the variable also $\tilde{Y}$ follows these oscillations. Lower values of $\tilde{Y}$ were expected for the ED potential with respect to the EAM one, due to an explicit energy dependence in the first case. This does not seem to be the case; however, note that for some shells (e.g., the fifth), although the displacement is larger for the ED potential, the local variable $\tilde{Y}_5$ is smaller.

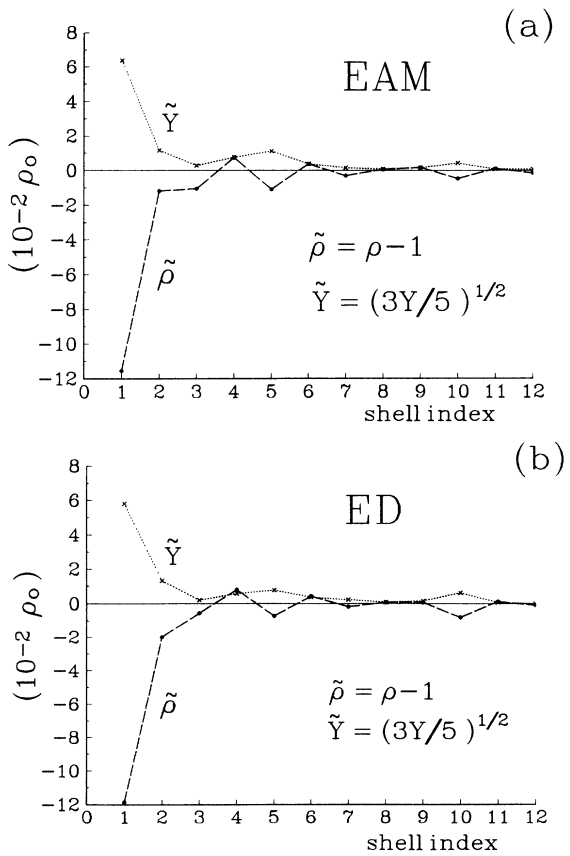

FIG. 3. Parameters $\tilde{\rho}$ (density change) and $\tilde{Y}$ for the vacancy, as a function of the shell index. (a) corresponds to the EAM potential and (b) to the ED one. ρ_0 is the equilibrum value of ρ.

Vacancy formation energies predicted by either potential are reported in Table IV, for the relaxed and unrelaxed configurations. Since an approximation to $E_f^{v,NR}$ [Eq. (7)] was one of the parameters used for fitting the potentials, the energies calculated for the unrelaxed lattice are very similar. After relaxation, the vacancy formation energy E_f^v is found to be smaller for the EAM potential than for the ED one, although the displacement patterns are similar. Previous calculated values of the vacancy formation energy using many-body potentials[12,13] approximately agree with our results, although we found that the E_f^v obtained with our EAM potential is somewhat smaller. As stated in the previous section, it is possible to separate many-body from pair contributions to the formation energy of the defects and to compute these contributions for each atomic site [see Eq. (13)]. The corresponding results are reported in Fig. 4 and Table IV. The table shows that, as a consequence of the value of ξ [Eq. (7)], the many-body contribution to E_f^v is much smaller for the EAM potential than for the ED one, where it comes mainly from the angular term. Actually, for either interatomic potential the energy contribution coming from the local density term F increases its value when the defect lattice is relaxed. The contribution of the effective pair interaction is the most important in both cases, and it is clearly the driving force of the relaxation, although for the ED potential the angular term contribution is significative. This is also seen in Fig. 4, where the contributions to E_f^v per atomic site (i.e., the difference in each energy term evaluated at the atomic site in the relaxed and perfect lattice configurations) are plotted for the effective pair interaction [Fig. 4(a)] and for the many-body terms [Fig. 4(b)] as a function of neighboring shell number. It can be seen that the contribution of the pair interaction is not only the most important one, but similar for both potentials. Note that the oscillations in Fig. 4(a) are not necessarily in direct correlation with those of the displacements (Fig. 2), contrary to what happens for density changes (Fig. 3). This is because the effective pair potential V of Eq. (9) is richer than the function Φ in functional details.

Finally, we have calculated the relaxation volume

TABLE IV. Vacancy formation energy E_f (eV) calculated with the EAM and ED potentials. E_p, E_ρ, and E_g are, respectively, the contributions of the pair interaction V, embedding function F, and the angular term G.

	EAM		ED	
	Unrelaxed	Relaxed	Unrelaxed	Relaxed
E_f	1.815	1.567	1.808	1.634
E_p	1.799	1.547	1.440	1.273
E_ρ	0.016	0.020	0.054	0.079
E_g			0.314	0.282

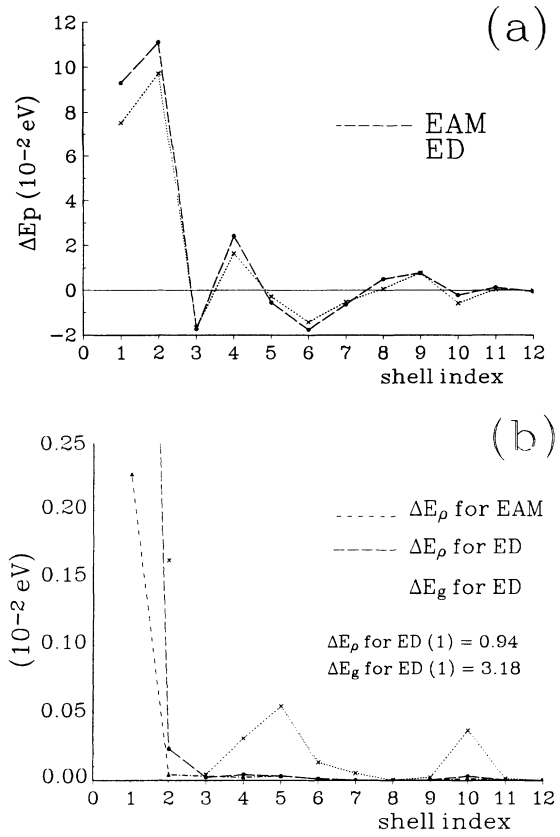

FIG. 4. Energy contributions V, F, and G of Eq. (1) at each atomic site, as a function of the shell index. (a) Effective pair contributions and (b) many-body contributions.

$\Delta V/\Omega$ for both potentials, using Eqs. (15) and (16). These results are presented in Table V ("computer simulation" row). We could not find experimental data on $\Delta V/\Omega$ for the vacancy in Fe. According to Harder and Bacon,[12] vacancy relaxation volumes are accepted to be in the range -0.2 to -0.1 for bcc metals. Those authors report the computer simulation result for the Fe N-body potential of Ref. 2, $\Delta V/\Omega = -0.15$, in agreement with our calculations.

B. Kanzaki forces and relaxation volume

The vacancy relaxation volume $\Delta V/\Omega$, being a measurable value of the defect-induced lattice relaxation, is an important parameter for comparing predictions of different interatomic potentials. In this section we give a brief description of the force field in the vicinity of the vacancy and focus on its relationship to the defect volume change.

We first calculate $\mathbf{K}^0$ of Eq. (25), i.e., the Kanzaki forces at the unrelaxed lattice. A detailed analysis is given in the Appendix. The expressions and numerical values obtained for the EAM and ED potentials are reported in Table VI. Those expressions are deduced for a vacancy in a bcc lattice when second-neighbor interactions are considered. It is seen that, for both potentials, the effective pair interaction provides an inward contribution to the forces for the first neighbors of the vacant site and an outward contribution for the second neighbors; the local density term $F(\rho_i)$ always contributes inwards, while the term $G(Y_i)$ does so mainly outwards, changing sign for the fifth and sixth neighbors. Note that the many-body terms induce forces reaching the sixth neighboring shell from the vacancy (twice the potential range).

The forces $\mathbf{K}^0$ are used for calculating the dipole tensor [Eq. (27)] and an approximated value for the vacancy relaxation volume. The resulting analytic expressions and the corresponding numerical values for both potentials are reported in Table V. Those expressions are obtained by replacing the $\mathbf{K}^0$ of Table VI in Eqs. (27) and (16). As mentioned before, the pair interaction term of our potentials constitutes by itself an *equilibrium* potential for the lattice with the correct lattice parameter. Therefore, if relaxation is not permitted, the contribution of the pair interaction to $\Delta V/\Omega$ is null (it would be proportional to minus the Cauchy pressure for a nonequilibrium pair potential). On the contrary, many-body terms can have a nonvanishing contribution, and within this approximation, they are the only terms responsible for the predicted volume change. In fact, the many-body term F provides a negative $\Delta V/\Omega$, while the angular term of the ED potential contributes with a positive volume change. In the approximation considered, a better agreement with the computer simulation results is expected for the ED potential than for the EAM one. This is due to the larger weight of the many-body terms as measured by the parameter ξ [Eq. (7)]: 0.2 for the former against 0.013 for the latter. Note that though G weights about 6 times more than F in the parameter ξ of the ED potential, its contribution to the defect volume change is only half of the contribution from F and of opposite sign. It is seen that the two terms add up to a negative relaxation volume which is in good agreement with the computer

TABLE V. Analytical expressions for the contributions to the vacancy volume change ($\Delta V/\Omega$) of the various energy terms in Eq. (1), obtained from Table VI, Eqs. (27) and (16), and the corresponding numerical values. Computer simulation calculations are also reported.

	$\Delta V/\Omega$	EAM	ED
Computer simulation, Eqs. (15) and (16)		-0.14	-0.11
Unrelaxed approximation			
from $V(R_{ij})$	$[8(\sqrt{3/2})V_1'+6V_2']/3B\Omega$	0.00	0.00
from $F(\rho_i)$	$-8[(7F_1'+6F_2')\phi_1'+(8F_1'+5F_2')\sqrt{3/2}\phi_2']/3B\Omega$	-0.05	-0.20
from $G(Y_i)$	$-\frac{32}{3}G_0'[\phi_1'\phi_1+(\sqrt{3/2})\phi_2'\phi_2]/3B\Omega$		0.10
Total		-0.05	-0.10

TABLE VI. Kanzaki's forces for the unrelaxed lattice with a vacancy. All forces are radial, except for the [3,1,1] shell. Numerical values in 10^{-2} eV/R_{1e}. Subindexes 1 and 2 refer to first and second neighbors of the vacant site, respectively. G' stands for the constant G'_0 of the text.

Shell	Force's expression	EAM	ED
	Pair term $[V(R_{ij})]$ contribution		
1 [1,1,1]	$V'_1[111]/\sqrt{3}$	−97.27	−77.28
2 [2,0,0]	$V'_2[100]$	112.32	89.24
	Embedding function $[F(\rho_i)]$ contribution		
1 [1,1,1]	$[(F'_1-F'_2)\phi'_1-\sqrt{3}F'_1\phi'_2][111]/\sqrt{3}$	−0.64	−1.05
2 [2,0,0]	$[(-4/\sqrt{3})F'_1\phi'_1+F'_2\phi'_2][100]$	−3.22	−16.65
3 [2,2,0]	$-\sqrt{2}[(2/\sqrt{3})F'_1\phi'_1+F'_2\phi'_2][110]/\sqrt{2}$	−3.23	−11.44
4 [3,1,1]	$-F'_2\phi'_1[111]/\sqrt{3}-F'_1\phi'_2[100]$	−[1.29,0.56,0.56]	−[5.79,1.57,1.57]
5 [2,2,2]	$-F'_1\phi'_1[111]/\sqrt{3}$	−1.59	−7.74
6 [4,0,0]	$-F'_2\phi'_2[100]$	−0.44	−1.23
	Angular term $[G(Y_i)]$ contribution		
1 [1,1,1]	$-\frac{4}{3}G'\phi_1(\phi'_1+7\phi_2/R_{1e})[111]/\sqrt{3}$		22.93
2 [2,0,0]	$-\frac{4}{3}G'[(4/3\sqrt{3})\phi'_1\phi_1+\phi'_2\phi_2$ $+(16/3\sqrt{3})\phi_1^2/R_{1e}][100]$		18.34
3 [2,2,0]	$-2\sqrt{2}G'[(4/9\sqrt{3})\phi'_1\phi_1+\phi'_2\phi_2/3$ $-(8/9\sqrt{3})\phi_1^2/R_{1e}][110]/\sqrt{2}$		35.96
4 [3,1,1]	$2\sqrt{\frac{2}{3}}G'\phi_1\phi_2/R_{1e}[411]/\sqrt{18}$		[3.18,0.80,0.80]
5 [2,2,2]	$\frac{4}{3}G'\phi'_1\phi_1[111]/\sqrt{3}$		−42.24
6 [4,0,0]	$\frac{4}{3}G'\phi'_2\phi_2[100]$		−7.50

simulation result [Eqs. (15) and (16)] also reported in Table V. The latter value is taken as the most accurate one due to the fact that the size of the simulation block employed guarantees a fairly converged figure. The mentioned agreement, however, may be fortuitous in view of the poor result obtained for the EAM potential in this approximation. Although we do not expect contributions to change sign, the more refined analysis proposed in Sec. III C is needed to compare with the computer results and to gain insight into the different potentials predictions. Results for the vacancy relaxation volume computed along these lines, using the zeroth, first, second, etc., approximation defined in Sec. III C, are given in Table VII. It is seen here that the zeroth approximation already gives a result close to the computer simulation for the EAM potential. However, for the ED potential higher-order approximations are needed, at least up to the fifth, which includes the second ⟨111⟩ neighboring shell. This result is consistent with the magnitude and distribution of the unrelaxed forces shown in Table VI: Forces are much bigger for the ED potential and decrease slower with distance than for the EAM potential.

TABLE VII. Vacancy relaxation volumes computed with the different approximations of Sec. III C for both EAM and ED potentials. Within parentheses is the neighboring shell included in the approximation (see text).

Order of approximation	$\Delta V/\Omega$ (EAM)	$\Delta V/\Omega$ (ED)
0	−0.154	−0.207
1 (⟨111⟩)	−0.129	−0.209
2 (⟨200⟩)	−0.133	−0.156
3 (⟨220⟩)	−0.132	−0.156
4 (⟨311⟩)	−0.133	−0.152
5 (⟨222⟩)	−0.130	−0.118
6 (⟨400⟩)	−0.130	−0.117

V. SELF-INTERSTITIALS

Formation energies and relaxation volumes are calculated for the ⟨110⟩ and ⟨111⟩ dumbbells; the results are presented in Table VIII. Contributions to E_f of the different interaction terms are reported separately. The eigenvalues of the corresponding dipole tensors P are also given in that table. The relaxed configurations of other possible interstitials are not recovered under the action of small perturbations; therefore, they are considered to be

TABLE VIII. Formation energies E_f (eV), dipole tensor eigenvaluesI P_i and relaxation volumes $\Delta V/\Omega$ of the interstitial configurations simulated with both potentials. E_p, E_ρ, and E_g are, respectively, the contributions of the interaction V, embedding function F, and the angular term G to E_f.

	⟨111⟩		⟨110⟩	
	EAM	ED	EAM	ED
E_f	4.34	4.66	4.15	4.36
E_p	4.23	3.88	4.04	3.59
E_ρ	0.11	0.08	0.11	0.11
E_g		0.70		0.66
P_1	24.8	41.9	19.4	28.1
P_2	10.0	16.9	10.2	17.0
P_3	10.0	16.9	16.8	26.2
$\Delta V/\Omega$	1.1	1.9	1.2	1.8

unstable and are not reported here.

It is seen that the ED potential gives higher values of E_f. Because of the angular term, the many-body contributions are more important for this potential than for the EAM one. Dipole tensor components are bigger for the ED potential, and therefore the relaxation volumes obtained are significantly higher. Note that P is slightly more isotropic for the ED potential, i.e., the relative differences between the three eigenvalues are smaller.

To the authors' knowledge, the only experimental result on self-interstitial configurations in Fe, obtained by a magnetic relaxation technique, is that the dumbbell $\langle 110 \rangle$ is the most stable one.[27] Besides this, only a few calculations are available. Johnson, using pair potentials,[15] reports formation energies of various configurations relative to the $\langle 110 \rangle$ dumbbell and their relaxation volumes. We found some of Johnson's configurations to be unstable, but the E_f's we obtained are consistent with the values reported by him, mainly those for the ED potential. More recently, Harder and Bacon[12] calculated formation energies and obtained the same relative stability of the different configurations as we do; however, the relaxation volume calculated by them for the $\langle 110 \rangle$ dumbbell is a little lower. Though experimental results on interstitials volume change are lacking, the values of $\Delta V/\Omega$ given by the ED potential seem to be too high when compared to the ones calculated for other bcc metals.[12,14]

VI. DISCUSSION

The ED method is an empirical extension of the EAM, in which a term depending on angles between neighboring atoms is added to the energy functional expression [Eq. (1)]. In this work we assume a linear dependence of the energy on the angular many-body variable Y, defined in Eq. (4).

One must remember that the EAM-type interatomic potentials retain the calculation simplicity of the pair interactions, but they allow the fitting of two important properties that were forbidden within the latter approximation.

(i) Independent values for the lattice cohesive energy and vacancy formation energy. For pair potentials these quantities are equal (except for the lattice relaxation); in the above EAM approach, where $F_0'=0$, these energies differ by a many-body term

$$E_f^{v,Nr}=|E_{\rm coh}|-|F_0|+AP_C \ ,$$

where no lattice relaxation is considered; F_0 is the perfect lattice value of the embedding function, P_C is the Cauchy pressure, and A is a density-dependent function, positively defined:

$$A=\Omega\frac{\sum_\nu N_\nu \Phi_\nu^2}{[\sum_\nu N_\nu R_\nu \Phi_\nu'/3]^2} \ .$$

Similarly, for the second-moment tight-binding approximation,[7]

$$E_f^{v,NR}=|E_{\rm coh}|-\tfrac{1}{2}|U_{\rm TB}^{(0)}| \ ,$$

where $U_{\rm TB}^{(0)}$ is an electronic energy, which depends on the perfect lattice bandwidth.

(ii) The lattice is held in equilibrium with the correct Cauchy discrepancy. EAM potentials can reproduce the elastic constants ($c_{12}\neq c_{44}$) if the Cauchy pressure is positive, $P_C=(c_{12}-c_{44})/2>0$, while equilibrium pair potentials always predict $c_{12}=c_{44}$. For the case of negative Cauchy pressure, the EAM approach imposes to select nonphysically valid shapes of the embedding function $F(\rho)$. The additional many-body term in the ED potential allows the fitting of the elastic constants even for the case of $P_C<0$ [see Eq. (8)].

It is known that several properties of bcc transition metals cannot be reproduced by pair potentials and that angular-dependent terms must be considered in the configurational energy, for instance, to reproduce the measured phonon dispersion curves.[28,29] Several authors developed EAM-type potentials for those metals.[2,5,30] Among the three bcc metals Fe, Nb, and Cr, chosen in Ref. 5 for the construction of empirical potentials, Fe is the one that more nearly satisfies the (mathematical) conditions to be approached by a pair interaction. Its Cauchy pressure P_C, which is a function related only to the derivatives of the many-body part of the energy, is positive. By contrast, P_C of Cr is negative, and that of Nb is larger than Fe's (0.107 eV/A^3 against 0.328 eV/A^3). In addition, the ratio between vacancy formation energy and cohesive energy in Fe is 0.42 against 0.29 in Cr and 0.26 in Nb. Therefore, on fitting an EAM potential for Fe, the many-body contribution is small, being the pair part the dominant one. On fitting the ED potential, we have imposed an arbitrary contribution of the many-body part to the energy. This was fixed as 20% of the (unrelaxed) formation energy of the vacancy. It is important to realize that although most of this contribution comes from the angular term G, the contribution of the term F also increases with respect to the one in the EAM approach.

We found that the bcc structure is more easily stabilized with the ED potential than with the EAM one. Note in Table III that the ED potential gives a higher value of $E_{\rm fcc}-E_{\rm bcc}$ ($E_{\rm fcc}$ is the cohesive energy of a fcc lattice with the lattice constant corresponding to the *minimum-energy fcc structure* found with each potential). Also, although the "unrelaxed" formation energy of the vacancy fitted by either potential is the same, after relaxation the vacancy is found to be "easier" to create (lower formation energy) in a lattice held by the EAM potential than in one held by the ED.

We shall analyze the calculated results for the vacancy in order to compare differences among the predictions of either interatomic potential. The displacement field induced by the defect was found to oscillate as the distance to the vacant site increases. This oscillation can either be a result of the elastic response of the material, as discussed by Tewary[17] regarding the Green function for a discrete lattice, or be related to the oscillatory character of the source forces discussed below. One of the features of the EAM-type interactions is that the many-body variables and each contribution to the local energy can be associated with a given lattice site [Eqs. (1), (3), and (4)]. Therefore density and energy variations as a function of

the atomic location can be studied. The density oscillations, as revealed by the parameter $\tilde{\rho}$ in Fig. 3, follow those of the displacement field (excluding the defect's closest neighbors). Such a result is to be expected, since density is determined mainly through distances between interacting shells and Φ is a decreasing function in all its range. EAM and ED results are quite similar.

Figure 4(b) shows that the many-body, density-dependent contribution $F(\rho)$ to the defect energy decays almost monotonically with distance from the vacancy. This contribution is smaller for the EAM potential than for the ED one, mainly because of the lower curvature of the corresponding embedding function. The angular contribution $G(Y)$ is more important than the one of the term F and has a richer structure, reflecting oscillations in the displacements [remember that in our approximation the term $G(Y)$ is linear in the angular many-body variable]. By far, the most important contribution to the energy relaxation comes from the pair interaction. The oscillations of this contribution with distance from the vacancy [Fig. 4(b)] do not follow those of the displacements, being determined both by the distances between interacting shells and by the shape of the effective pair function.

The harmonic response of a lattice to a point-defect force source was discussed in Sec. III above. Regarding the vacancy, the Kanzaki forces $\mathbf{K}^0$ at the unrelaxed configuration are analytically evaluated (Table VI). As detailed in the Appendix, the forces on any atom coming from the many-body terms $F(\rho)$ and $G(Y)$ can be thought as composed by two contributions: one due to the fact that when the atom considered moves, its own ρ_i or Y_i is varied ("self-force") and the other one due to the variation of the ρ_j or Y_j of its neighbors. The first contribution to $F(\rho)$ takes the atom away from the vacancy toward the bulk material, while the second gives a net force toward the vacancy. A similar situation holds for the angular term $G(Y)$ regarding the first contribution, the balance for the second being a little more involved though producing a mainly outward effect. This is a new feature with respect to the simple EAM model. Compared to the EAM potential, such an effect is responsible for a smaller vacancy relaxation volume. Ohta *et al.*[31] calculated the force field around the unrelaxed vacancy in several bcc metals using the tight-binding bond (TBB) model. This is a more sophisticated approach to atomic cohesion than either the EAM or ED ones. Some features of that work resemble the results obtained with the ED potential, particularly the large many-body force toward the vacancy acting on the fifth neighbors, though we do not expect to reproduce their result of a significant force on the second neighbors toward the vacancy (only the term F contributes in this sense in our model).

In Ref. 31, Ohta *et al.* described the vacancy relaxation in terms of the strengthening of bonds connecting atoms near the defect. This description is somewhat ill defined within our model because for the many-body contributions energy is associated with atomic sites rather than with bonds. Nevertheless, as discussed by Carlsson,[7] either within a second-moment tight-binding approximation or the EAM formalism, an environment-dependent effective pair interaction can be defined [Eq. (5.14) in Ref. 7] in the same fashion as the effective pair for the perfect lattice. This interaction adds an attractive term for lower coordination numbers than the bulk; therefore, the effect of introducing a vacancy could be interpreted as a strengthening of the bonds in the vicinity of the vacancy. However, Carlsson's description of the vacancy relaxation can be misleading because of his restriction to a first-neighbor interaction. An equilibrium first-neighbor pair interaction does not relax the single vacancy (neither a vacancy cluster nor the free surface). Within the above models, as long as the effective pair interaction reaches more than first neighbors—and this is likely to be the case for bcc materials—the driving force of the relaxation may not be bond strengthening. In fact, in our case this effect is minor (as reflected in Table VI) for the unrelaxed vacancy forces: The contribution of the effective pair term on the first two neighbors is much larger than either of the many-body ones.

The values obtained for the relaxation of the vacancy, the "computer simulation" row of Table V, are consistent with experimental results and previous computer simulations in bcc metals.[12] We have found that the volume change computed by means of the unrelaxed force pattern may not be a good approximation, as shown by the "total unrelaxed" row of Table V. This procedure is equivalent to the zeroth approximation proposed by Maysenhölder[32] for the case of Finnis and Sinclair's (FS) potentials.[2] His results show, however, a poor agreement with the fully relaxed volume changes reported in Ref. 12 calculated with the same potentials. Moreover, we have found that even for a simple defect such as a vacancy, anharmonic effects can be important. In this sense, the EAM potential shows only a mild anharmonicity and the zeroth approximation of Table VII already gives a fair value for the volume change. On the other hand, for the ED potential with a rather similar displacement pattern as the EAM, no convergency to the computer simulation result is reached until the vacancy core is "augmented" to include the fifth neighbors of the missing atom (fifth row of Table VII). This fact is related to the big contribution of the angular term to the unrelaxed forces on the fifth neighboring shell (see Table VI). Therefore the core region of the vacancy is much more extended for the ED potential than for the EAM one.

Regarding the interstitial configurations, it was found that both the EAM and ED potentials reproduce the minimum energy dumbbell configuration, i.e., the $\langle 110 \rangle$. Compared to the results obtained with the EAM potential, the ED model gives higher formation energies and relaxation volumes. To the authors' knowledge, the only experimental interstitial relaxation volume reported for a bcc metal is the one corresponding to the $\langle 110 \rangle$ dumbbell in Mo:[33] about 1.1 at. vol. This value and those calculated for several bcc metals[12] using FS potentials[2] are considerably lower than the results given by the ED potential. This is consistent with a more extended core region given by the latter potential, since forces induced by the defect in this region are expected to be mainly outwards rather than oscillating. However, it must be kept in mind that as the displacements produced by intersti-

tials are larger than those produced by a vacancy (up to ~20% of the equilibrium first-neighbor distance), the linear dependence of the energy on the angular variable Y may be open to question. In addition to the larger relaxation volume obtained with the ED model, a smaller anisotropy in the eigenvalues of the dipole tensor P is found. As a consequence, volume-dependent defect interactions are predicted to increase and the ones depending on the anisotropy of P will decrease, with respect to EAM predictions. A more detailed analysis of the interstitial configurations will be reported elsewhere.

We conclude that even though the overall features of the lattice relaxation induced by the simulated defects can be dominated by the effective pair part of the interactions, when many-body angular-dependent forces are introduced, the defect cores are revealed to be different from the ones calculated with the EAM potential. The differences are minor if only displacements are analyzed, but they become apparent when the anharmonic part of those displacements is studied, as done above.

Regarding the empirical interatomic potentials used in this work, we can say that both of them are appropriate for computer simulation of defects. The ED approximation, which is more sensitive to the atomic environment than the EAM one, seems to be physically more valid for relatively small displacements, but it may enhance too much the anharmonic features of the defect. On the other hand, the EAM potential is slightly less stable, supporting the general notion that in bcc transition metals stability is favored by many-body angular-dependent interactions.[8]

ACKNOWLEDGMENTS

This work was supported by Consejo Nacional de Investigaciones Científicas y Técnicas (CONICET) and Proyecto Multinacional de Materiales (Organización de Estados Americanos–Comisión Nacional de Energía Atómica), Argentina.

APPENDIX

The α component of the total force on any atom i of the lattice is

$$F_i^\alpha = -\frac{\partial E_{\rm tot}}{\partial x_i^\alpha} = \sum_{i\neq j} F_{ij}^\alpha[V] + F_{ij}^\alpha[F] + F_{ij}^\alpha[G] \ , \tag{A1}$$

where $E_{\rm tot}$ is the total energy of the crystal and

$$F_{ij}^\alpha[V] = -V'(R_{ij}) r_{ij}^\alpha \ , \tag{A2}$$

$$F_{ij}^\alpha[F] = [F'(\rho_i) + F'(\rho_j)]\Phi'(R_{ij}) r_{ij}^\alpha \ , \tag{A3}$$

$$F_{ij}^\alpha[G] = -4\sum_{\beta=1}^{3} \frac{\Phi(R_{ij})}{R_{ij}} [G_i' D_i^{\alpha\beta} + G_j' D_j^{\alpha\beta}] r_{ij}^\beta - 2\sum_{\beta,\gamma=1}^{3} \left[\Phi'(R_{ij}) - 2\frac{\Phi(R_{ij})}{R_{ij}} \right] \times [G_i' D_i^{\beta\gamma} + G_j' D_j^{\beta\gamma}] r_{ij}^\beta r_{ij}^\gamma r_{ij}^\alpha \tag{A4}$$

are the contributions to F_i^α of the different terms in the energy expansion [Eq. (1)] corresponding to the interaction with neighbor j. In the preceding equations, r_{ij}^α is the α component of a unit vector pointing from atom i to atom j and $D_i^{\alpha\beta}$ stands for the $\alpha\beta$ component of the deviatoric part of tensor λ_i.

The first term on the right in Eq. (A3) is a contribution to what we have called the "self-force" in the text, due to the fact that when the atom moves, its own density is varied, while the second term is due to the variation of the density of the neighbor j. For the angular forces [Eq. (A4)], self-force terms are those containing G_i', while the neighbor contribution is given by terms in G_j'. Note that $\Phi' < 0$ and, for densities appropriate for the vacancy, $F'(\rho) < 0$. Therefore Eq. (A3) represents an attractive force between atoms i and j ("bond strengthening").

The different contributions to the unrelaxed Kanzaki forces of Eq. (25) are reported in Table VI. We shall exemplify the derivation of those expressions calculating the Kanzaki forces for the atom labeled 0 in Fig. 5 (first neighbor of the vacancy v). We shall use the symbol $\mathbf{K}_{0k}[X]$ to indicate the force on 0 due to atoms k coming from source X ($X = V, F, G$); a sum over atoms with the same label in Fig. 5 is implied in this definition. The contribution of X ($X = F, G$) to the self-force will be noted as $\mathbf{K}_{00}[X]$.

The pair interaction only contributes a repulsive term from atom 1", namely,

$$\mathbf{K}_{01''}[V] = V'(R_1)\frac{[111]}{\sqrt{3}} \ , \quad V'(R_1) < 0 \ , \tag{A5}$$

where R_1 is the first-neighbor distance ($R_1 = R_{1e}$ since the atoms are at their perfect lattice positions).

The embedding function contributions are

$$\mathbf{K}_{00}[F] = F'(\rho_0)\Phi'(R_1)\frac{[111]}{\sqrt{3}} \ , \tag{A6a}$$

$$\mathbf{K}_{01'}[F] = -F'(\rho_{1'})\Phi'(R_1)\frac{[111]}{\sqrt{3}} \ , \tag{A6b}$$

$$\mathbf{K}_{02'}[F] = -\sqrt{3}F'(\rho_{2'})\Phi'(R_2)\frac{[111]}{\sqrt{3}} \quad (\rho_{2'} = \rho_0) \ , \tag{A6c}$$

and $\mathbf{K}_{0k}[F] = 0$ for the remaining k's. R_2 is the second-neighbor distance.

Finally, the contribution from the term G is given by

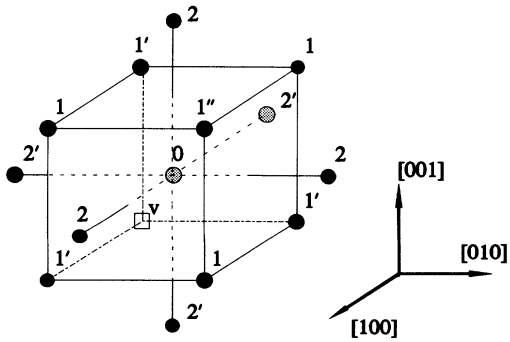

FIG. 5. Vicinity of the vacancy relevant for the unrelaxed forces calculation.

replacing $G_i'=G_j'=G_0'$ in Eq. (A4),

$$\mathbf{K}_{00}[G]=-\frac{4}{3}G_0'\Phi(R_1)\Phi'(R_1)\frac{[111]}{\sqrt{3}}\ , \tag{A7a}$$

$$\mathbf{K}_{01'}[G]=-\frac{16}{3}G_0'\frac{\Phi(R_1)\Phi(R_2)}{R_1}\frac{[111]}{\sqrt{3}}\ , \tag{A7b}$$

$$\mathbf{K}_{02'}[G]=-4G_0'\frac{\Phi(R_1)\Phi(R_2)}{R_1}\frac{[111]}{\sqrt{3}}\ , \tag{A7c}$$

and $\mathbf{K}_{0k}[G]=0$ for the remaining k's.

Note the force balance in Eqs. (A6) and (A7): Equations (A6a) and (A7a) are positive along [111], while Eqs. (A6b), (A6c), (A7b), and (A7c) are negative.

[1]M. S. Daw and M. I. Baskes, Phys. Rev. B **29**, 6443 (1984).
[2]M. W. Finnis and J. E. Sinclair, Philos. Mag. A **50**, 45 (1984).
[3]F. Ercolessi, E. Tosatti, and M. Parrinello, Phys. Rev. Lett. **57**, 719 (1986).
[4]M. I. Baskes, J. S. Nelson, and A. F. Wright, Phys. Rev. B **40**, 6085 (1989).
[5]R. Pasianot, D. Farkas, and E. J. Savino, Phys. Rev. B **43**, 6952 (1991); **47**, 4149(E) (1993).
[6]A. E. Carlsson, Phys. Rev. B **44**, 6590 (1991).
[7]A. E. Carlsson, in *Solid State Physics: Advances in Research and Applications,* edited by H. Ehrenreich and D. Turnbull (Academic, New York, 1990), Vol. 43, p. 1.
[8]J. R. Smith and D. J. Srolovitz, Modelling Simulation Mater. Sci. Eng. **1**, 101 (1992).
[9]M. I. Baskes, Phys. Rev. Lett. **59**, 2666 (1987).
[10]M. I. Baskes, Phys. Rev. B **46**, 2727 (1992).
[11]G. Simonelli, R. Pasianot, and E. J. Savino, in *Materials Theory and Modelling,* edited by P. D. Bristowe, J. Broughton, and J. M. Newsam, MRS Symposia Proceedings No. 291 (Materials Research Society, Pittsburgh, 1993), p. 567.
[12]J. M. Harder and D. J. Bacon, Philos. Mag. A **54**, 651 (1986).
[13]A. M. Guellil and J. B. Adams, J. Mater. Res. **7**, 639 (1992).
[14]R. A. Johnson, Phys. Rev. B **27**, 2014 (1983).
[15]R. A. Johnson, Phys. Rev. **134**, A1329 (1964).
[16]E. J. Savino and D. Farkas, Philos. Mag. A **58**, 227 (1988).
[17]V. K. Tewary, Adv. Phys. **22**, 757 (1973).
[18]J. H. Rose, J. R. Smith, F. Guinea, and J. Ferrante, Phys. Rev. B **29**, 2963 (1984).
[19]C. Kittel, *Introduction to Solid State Physics,* 4th ed. (Wiley, New York, 1971).
[20]J. P Hirth and J. Lothe, *Theory of Dislocations,* 2nd ed. (Wiley, New York, 1982).
[21]G. J. Ackland, G. Tichy, V. Vitek, and M. W. Finnis, Philos. Mag. A **56**, 735 (1987).
[22]M. J. Norgett, R. C. Perrin, and E. J. Savino, J. Phys. F **2**, L73 (1972).
[23]H. R. Schober and K. W. Ingle, J. Phys. F **10**, 575 (1980).
[24]G. Leibfried and N. Breuer, *Point Defects in Metals I,* Springer Tracts in Modern Physics (Springer, Berlin, 1978).
[25]P. A. Flinn and A. A. Maradudin, Ann. Phys. (N.Y.) **18**, 81 (1962).
[26]H. Kanzaki, J. Phys. Chem Solids **2**, 24 (1957).
[27]W. Chambron, J. Verdone, and P. Moser, *Fundamental Aspects of Radiation Damage in Metals,* edited by M. T. Robinson and F. W. Young (NTIS, U.S. Department of Commerce, 1975), Vol. I, p. 261.
[28]V. P. Singh, H. L. Kharoo, M. Kumar, and M. P. Hemkar, Nuovo Cimento B **32**, 40 (1976).
[29]B. A. Oli and A. O. E. Animalu, Phys. Rev. B **13**, 2398 (1976).
[30]R. A. Johnson and D. J. Oh, J. Mater. Res. **4**, 1195 (1989).
[31]Y. Otha, M. W. Finnis, D. G. Pettifor, and A. P. Sutton, J. Phys. F **17**, L272 (1987).
[32]W. Maysenhölder, Philos. Mag. A **53**, 783 (1986).
[33]P. Ehrhart, J. Nucl. Mater. **69&70**, 200 (1978).

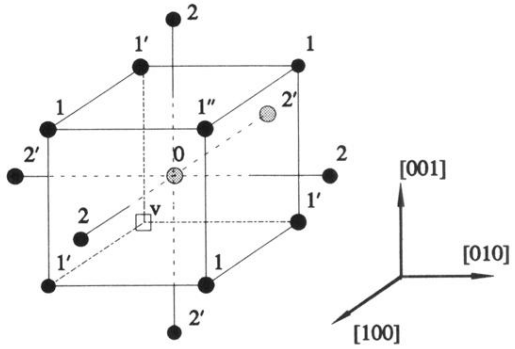

FIG. 5. Vicinity of the vacancy relevant for the unrelaxed forces calculation.